LETTER

doi:10.1038/nature12138

Macropinocytosis of protein is an amino acid supply route in Ras-transformed cells

Cosimo Commisso[1], Shawn M. Davidson[2]*, Rengin G. Soydaner-Azeloglu[1]*, Seth J. Parker[3]*, Jurre J. Kamphorst[4], Sean Hackett[4], Elda Grabocka[1], Michel Nofal[4], Jeffrey A. Drebin[5], Craig B. Thompson[6], Joshua D. Rabinowitz[4], Christian M. Metallo[3], Matthew G. Vander Heiden[2,7] & Dafna Bar-Sagi[1]

Macropinocytosis is a highly conserved endocytic process by which extracellular fluid and its contents are internalized into cells through large, heterogeneous vesicles known as macropinosomes. Oncogenic Ras proteins have been shown to stimulate macropinocytosis but the functional contribution of this uptake mechanism to the transformed phenotype remains unknown[1–3]. Here we show that Ras-transformed cells use macropinocytosis to transport extracellular protein into the cell. The internalized protein undergoes proteolytic degradation, yielding amino acids including glutamine that can enter central carbon metabolism. Accordingly, the dependence of Ras-transformed cells on free extracellular glutamine for growth can be suppressed by the macropinocytic uptake of protein. Consistent with macropinocytosis representing an important route of nutrient uptake in tumours, its pharmacological inhibition compromises the growth of Ras-transformed pancreatic tumour xenografts. These results identify macropinocytosis as a mechanism by which cancer cells support their unique metabolic needs and point to the possible exploitation of this process in the design of anticancer therapies.

To date, the induction of macropinocytosis by oncogenic Ras has been characterized in the setting of overexpressed proteins[1–3]. To determine whether stimulated macropinocytosis is a feature of cancer cells endogenously expressing oncogenic Ras, we analysed fluid-phase uptake in human pancreatic and urinary bladder cancer cell lines harbouring oncogenic Ras mutations and compared uptake to wild-type Ras-expressing cells originating from carcinomas of the same tissue type. Macropinosomes were visualized on the basis of the ability of cells to internalize extracellular medium containing tetramethylrhodamine-labelled high-molecular-mass dextran (TMR-dextran), an established marker of macropinocytosis. Pancreatic adenocarcinoma-derived human MIA PaCa-2 cells, which are homozygous for the $KRAS^{G12C}$ allele[4], displayed appreciably higher levels of TMR-dextran uptake compared to BxPC-3 cells, which express wild-type *KRAS*[5] (Fig. 1a, b). That the TMR-dextran labelling in the oncogenic Ras-expressing cells reflects uptake through macropinocytosis is indicated by the observation that uptake was inhibited in a dose-dependent manner by 5-(*N*-ethyl-*N*-isopropyl)amiloride (EIPA) (Fig. 1c, d), which has been shown to inhibit macropinosome formation without affecting other endocytic pathways[6,7]. Importantly, the knockdown of KRAS led to an attenuation of macropinocytosis, confirming the dependence of this uptake mechanism on oncogenic Ras expression (Supplementary Fig. 1a–d). This conclusion is further supported by the observation that bladder carcinoma-derived T24 cells, which are homozygous for the $HRAS^{G12V}$ allele[8], exhibit increased levels of macropinocytosis relative to 5637 cells, which express wild-type *HRAS* (Supplementary Fig. 2a–c)[9].

To examine whether oncogenic Ras-expressing cells engage in macropinocytosis *in vivo*, we used both a heterotopic xenograft mouse model and an autochthonous mouse model. For the heterotopic model, tumours were injected with fluorescein isothiocyanate-conjugated dextran (FITC-dextran) and intracellular uptake was

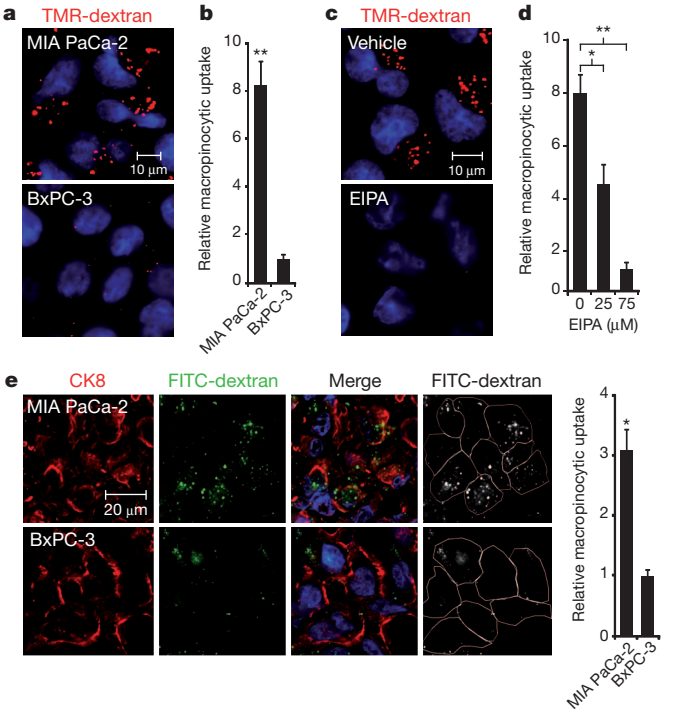

Figure 1 | Oncogenic KRAS-expressing pancreatic cancer cells display increased levels of macropinocytosis both in culture and *in vivo*. **a**, A macropinocytosis uptake assay using TMR-dextran as a marker of macropinosomes (red) indicates that MIA PaCa-2 cells display increased levels of macropinocytosis compared to BxPC-3 cells. DAPI (4′,6-diamidino-2-phenylindole) staining (blue) identifies nuclei. **b**, Quantification of macropinocytic uptake in pancreatic cancer cells. Data are expressed as arbitrary units and are presented relative to the values obtained for BxPC-3 cells. **c**, Macropinocytic uptake in MIA PaCa-2 cells treated with either vehicle (dimethylsulphoxide (DMSO)) or 75 μM EIPA. **d**, Quantification of macropinocytic uptake in MIA PaCa-2 cells treated with 0, 25 or 75 μM EIPA. Data are presented relative to the values obtained for the 75 μM condition. **e**, Visualization and quantification of macropinocytosis *in vivo*. Representative images from sections of FITC-dextran (green)-injected tumour xenografts stained with anti-CK8 (red). Cell boundaries (white outline) were delineated on the basis of CK8 staining. Data are presented relative to the values obtained for the BxPC-3 tumours. For all graphs, error bars indicate mean ± s.e.m. for $n = 3$ independent experiments with at least 300 cells scored per experiment. Statistical significance was determined by Student's *t*-test; $^*P < 0.05$, $^{**}P < 0.01$.

[1]Department of Biochemistry and Molecular Pharmacology, New York University School of Medicine, New York, New York 10016, USA. [2]Koch Institute for Integrative Cancer Research and Department of Biology, Massachusetts Institute of Technology, Cambridge, Massachusetts 02139, USA. [3]Department of Bioengineering, University of California, San Diego, La Jolla, California 92093, USA. [4]Lewis-Sigler Institute for Integrative Genomics, Carl Icahn Laboratory, Princeton University, Princeton, New Jersey 08544, USA. [5]Department of Surgery, Hospital of the University of Pennsylvania, Philadelphia, Pennsylvania 19104, USA. [6]Cancer Biology and Genetics Program, Memorial Sloan-Kettering Cancer Center, New York, New York 10065, USA. [7]Dana-Farber Cancer Institute, Boston, Massachusetts 02115, USA.

*These authors contributed equally to this work.

assessed by fluorescent microscopy of tissue sections. The number of macropinosomes identified as FITC-positive puncta was markedly higher in tumours derived from MIA PaCa-2 cells relative to BxPC-3-derived tumours (Fig. 1e). To confirm that the macropinosomes are a feature of the transplanted cells rather than the host cells, the tumour sections were stained with anti-CK8 antibody, which selectively labels the transplanted human epithelial cells[10] (Fig. 1e). To analyse macropinocytosis in mouse pancreatic tumours, we used an autochthonous mouse model of pancreatic cancer[11]. In this model, animals of the genotype *P48-cre; lsl-Kras^{G12D}; Trp53$^{-/+}$* (KPC) develop pancreatic intraepithelial neoplasia lesions within 4 weeks of birth and progress to invasive pancreatic ductal adenocarcinoma between 9 and 13 weeks[12]. To assess macropinocytic uptake, KPC mice were injected with FITC-dextran at 12 weeks of age and pancreata were subsequently collected. FITC-positive macropinosomes were detected in CK19-labelled acinoductal cells within mid- to late-stage pancreatic intraepithelial neoplasia lesions of KPC pancreata but not in pancreata from wild-type mice (Supplementary Fig. 3). Altogether, these data indicate that an increased level of macropinocytosis is an attribute of cancer cells expressing oncogenic Ras both *in vitro* and *in vivo*.

In mammals, approximately 70% of the soluble substances found in extracellular fluid can be accounted for by proteins, with serum albumin being the most abundant[13]. Therefore, we sought to determine whether protein uptake through macropinocytosis can be used by oncogenic Ras-expressing cells to meet their metabolic needs for proliferation. As an experimental system, we used oncogenic *Kras*-transformed mouse NIH 3T3 cells because of their documented dependence on glutamine[14]. The expression of oncogenic Kras^{V12} in these cells was sufficient to stimulate a robust EIPA-sensitive macropinocytic response as measured by TMR-dextran uptake (Fig. 2a, b). To monitor the internalization of albumin, NIH 3T3 Kras^{V12} cells were incubated with a FITC-labelled form of bovine serum albumin (FITC-BSA). As shown in Fig. 2c, FITC-BSA was incorporated into discrete intracellular structures that co-localized with TMR-dextran. Similar uptake was also observed in MIA PaCa-2 and T24 cells (Supplementary Fig. 4), indicating that albumin internalization can occur through macropinocytosis in cancer cells harbouring endogenous oncogenic Ras mutations. Inhibition of FITC-BSA uptake by treatment with EIPA confirmed that the uptake mechanism was macropinocytosis (Fig. 2d).

The macropinocytic internalization and subsequent degradation of albumin could in principle lead to the generation of amino acids that sustain tumour cell bioenergetics and macromolecular synthesis[15]. To determine whether the internalized albumin is intracellularly degraded, we used a highly self-quenched BODIPY-dye-conjugated form of BSA (DQ-BSA) that emits a bright fluorescent signal only after proteolytic digestion[16]. Dual labelling of cells with DQ-BSA and TMR-dextran was used to establish the macropinocytic origin of the degradative compartment. In NIH 3T3 Kras^{V12} cells that were immediately fixed following a 30-min incubation with DQ-BSA and TMR-dextran ($t = 0$), there was no appreciable DQ-BSA fluorescence detected in macropinosomes (Fig. 2e). However, in cells that were incubated for 30 min and subsequently chased for 1 h in media free of both DQ-BSA and TMR-dextran, DQ-BSA fluorescence was detected in TMR-positive macropinosomes (Fig. 2e). DQ-BSA fluorescence was also detected within macropinosomes after a 1-h chase in MIA PaCa-2 and T24 cells, indicating that these trafficking events were also occurring in cancer cells harbouring endogenous oncogenic Ras mutations (Supplementary Fig. 5). The degradation of macropinocytosed albumin was dependent on lysosomal hydrolases, as treatment of MIA PaCa-2 and NIH 3T3 Kras^{V12} cells with bafilomycin A1 prevented the degradation of DQ-BSA (Supplementary Fig. 6). These data demonstrate that oncogenic Ras-expressing cells can harness macropinocytosis for the internalization and degradation of extracellular albumin, and raise the possibility that plasma protein degradation may provide an important source of intracellular amino acids.

Glutamine is a key nutrient for many proliferating cells and is metabolized to glutamate and then α-ketoglutarate to enter central carbon metabolism[17]. Ras-transformed cells exhibit an increased dependency on glutamine for growth and survival[14,18]. To test whether the degradation of macropinocytosed albumin results in the production of intracellular glutamine, we directly measured the intracellular concentrations of glutamate and α-ketoglutarate in cells grown either in the absence or presence of albumin. NIH 3T3 Kras^{V12} cells were cultured for 24 h in complete media supplemented with physiological concentrations of albumin (2 g per 100 ml, 2%). As a control, NIH 3T3 Kras^{V12} cells were grown in complete media alone. The addition of albumin to the media led to EIPA-sensitive increases in intracellular concentrations of both glutamate and α-ketoglutarate (Supplementary Fig. 7), indicating that macropinocytic uptake of albumin can increase the levels of glutamate and α-ketoglutarate in oncogenic Ras-transformed cells.

NIH 3T3 Kras^{V12} cells use glutamine as a main carbon source for tricarboxylic acid (TCA) cycle anaplerosis[19]. Therefore, to directly trace the fate of protein-derived amino acids in oncogenic Ras-transformed cells, we cultured NIH 3T3 Kras^{V12} cells in the presence of soluble, heat-inactivated, ^{13}C-labelled yeast protein. Uptake of

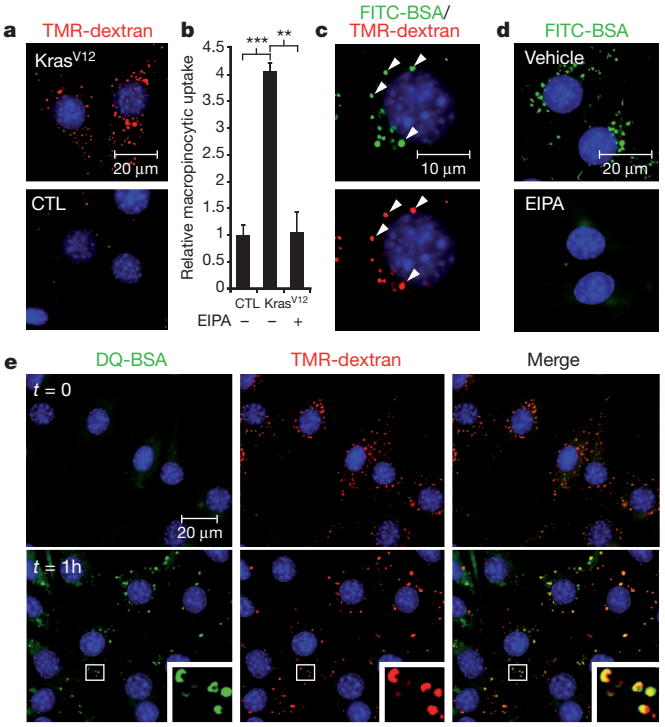

Figure 2 | Oncogenic Kras-induced macropinocytosis in mouse NIH 3T3 cells mediates the internalization of extracellular albumin, which is subsequently targeted for proteolytic degradation. **a**, TMR-dextran (red) is internalized at higher levels in NIH 3T3 Kras^{V12} cells (Kras^{V12}) compared to untransformed control cells (CTL). **b**, Quantification of macropinocytic uptake in control cells and NIH 3T3 Kras^{V12} cells incubated with vehicle (DMSO) or with 75 μM EIPA. Data are presented relative to the values obtained for the untransformed control cells. Error bars indicate mean ± s.e.m. for $n = 3$ independent experiments with at least 300 cells scored per experiment. Statistical significance was determined by Student's *t*-test; $^{**}P < 0.01$, $^{***}P < 0.001$. **c**, FITC-BSA (green) is internalized into discrete puncta that co-localize (white arrowheads) with TMR-dextran (red). **d**, FITC-BSA uptake is abrogated by treatment with 75 μM EIPA. **e**, Analysis of DQ-BSA fluorescence in NIH 3T3 Kras^{V12} cells that were co-incubated with DQ-BSA (green) and TMR-dextran (red) and fixed either immediately ($t = 0$) or following a 1-h chase. The fluorescent signal emanating from DQ-BSA ($t = 1$ h) is an indication of albumin degradation. Insets represent a higher magnification of the boxed areas. Images shown in **c**–**e** are representative of at least three independent experiments.

yeast-derived protein through macropinocytosis was confirmed microscopically by the fluorescent co-localization of rhodamine-labelled protein and FITC-dextran (Fig. 3a). After 24 h of culture in low-glutamine (0.2 mM) complete medium supplemented with ^{13}C-labelled yeast proteins, intracellular metabolites were extracted and ^{13}C labelling was quantified using gas chromatography/mass spectrometry (Supplementary Table 1)[20]. Substantial labelling of numerous intracellular amino acids, including glutamine, was detected (Fig. 3b), whereas only low levels of ^{13}C amino acids were detected in media samples incubated for the same period of time without cells (Supplementary Fig. 8). Catabolized yeast protein also entered central metabolism, as evidenced by ^{13}C-labelling of pyruvate, lactate and various TCA metabolites (Fig. 3c, d). Partially labelled mass isotopomers in numerous metabolites suggested that protein-derived amino acids were potentially being metabolized through several pathways, including glutamine anaplerosis/oxidation, acetyl-coenzyme A metabolism, reductive carboxylation and serine/glycine cycling (Fig. 3d and Supplementary Fig. 9).

Increased sensitivity to glutamine deprivation is a hallmark of cancer cells that express oncogenic mutants of Ras[14,18]. Consistent with this phenotype, we found that MIA PaCa-2, T24 and NIH 3T3 Kras^{V12} cells exhibited decreased proliferation at sub-physiological levels of glutamine as measured using the MTT viability assay or by Syto 60 staining (Supplementary Figs 10 and 11). We next examined whether cell growth impairment due to glutamine deprivation could be reversed by culturing cells in the presence of physiological levels of albumin. Albumin supplementation of media containing sub-physiological glutamine concentrations enhanced proliferation, and this effect was abrogated by EIPA treatment (Fig. 4a and Supplementary Fig. 11). The anti-proliferative response to EIPA observed in these settings was rescued by the addition of either extracellular glutamine or α-ketoglutarate (Fig. 4b). The ability of extracellular albumin to suppress the detrimental effects of glutamine starvation in MIA PaCa-2 cells was dependent on KRAS expression, as KRAS knockdown in these cells diminished the rescuing capacity of albumin (Supplementary Fig. 12). Together, these data indicate that the macropinocytic uptake of albumin could serve to sustain proliferation of oncogenic Ras-transformed cells by constituting a source of glutamine, and potentially other amino acids.

To investigate whether the uptake and degradation of albumin is a unique feature of oncogenic Ras-induced macropinocytosis, we used NIH 3T3 cells expressing Src^{Y527F} (NIH 3T3 Src^{Y527F}), a constitutively active form of Src[21]. Consistent with previous reports[22–24],

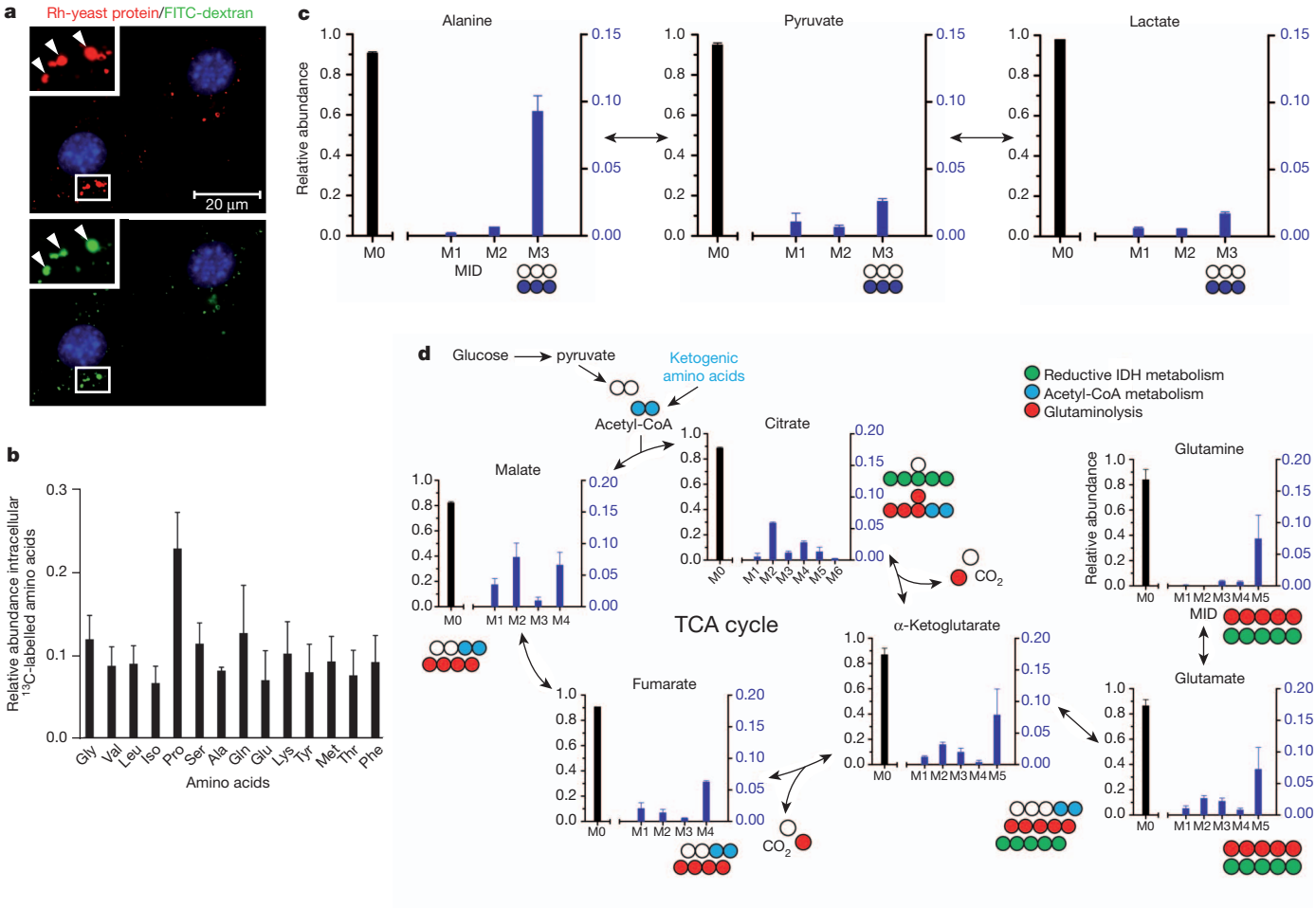

Figure 3 | Macropinocytic uptake of extracellular protein drives the accumulation of catabolic intermediates and entry of protein-derived amino acids into central carbon metabolism. **a**, Rhodamine (Rh)-labelled yeast protein (red) is internalized into puncta (arrowheads) that co-localize with FITC-dextran (green). Insets represent a higher magnification of the boxed areas. **b**, Uniformly ^{13}C-labelled intracellular amino acid pools were detected in NIH 3T3 Kras^{V12} cells after culture in low-glutamine-containing medium (0.2 mM) supplemented with 2% ^{13}C-labelled yeast protein. **c**, Protein-derived alanine enters central carbon metabolism upon transamination to pyruvate, and pyruvate can be directly converted to lactate. M3 reflects fully labelled alanine, pyruvate and lactate, whereas M0 abundances reflect metabolites with no ^{13}C label. M1 and M2 represent partially labelled species that are not present in substantial amounts. **d**, Atom-transition map depicting a model for the entry of amino-acid-derived carbons into the TCA cycle and isotopic labelling of various metabolites. Open circles represent unlabelled carbon, and different-coloured circles highlight labelling patterns that correspond to specific pathways as indicated in key. For all graphs, error bars indicate mean ± s.d. for three independent experiments. IDH, isocitrate dehydrogenase; MID, mass isotopomer distribution.

NIH 3T3 Src^{Y527F} cells displayed increased levels of macropinocytosis relative to untransformed control cells (Supplementary Fig. 13a). Moreover, Src-induced macropinosomes displayed the capacity to internalize and degrade extracellular albumin (Supplementary Fig. 13b). Importantly, the decrease in proliferation of Src-transformed cells following glutamine deprivation (Supplementary Fig. 10) could be rescued by extracellular albumin (Supplementary Fig. 13c), suggesting that the use of albumin by cancer cells to augment amino acid supply can be mediated by inducers of macropinocytosis other than Ras.

The above observations implicate macropinocytosis in providing nutrients to sustain cancer cell proliferation; therefore we sought to directly evaluate the role of macropinocytosis in tumour growth. Mice bearing MIA PaCa-2-derived heterotopic tumours were treated with EIPA or vehicle using an osmotic pump. EIPA administration commenced when tumours attained an average volume of 50–100 mm^3. After 7 days of treatment, FITC-dextran was delivered intratumorally and the tumours were excised. Tumour tissue collected from EIPA-treated animals displayed a reduction in macropinocytic uptake of FITC-dextran compared to vehicle-only controls (Fig. 4c). Moreover, relative to control tumours, those from EIPA-treated animals displayed an attenuation in growth and, in some cases regression (Fig. 4d, e). By contrast, EIPA administration had no effect on the growth rate of tumours derived from BxPC-3 cells, which display low levels of macropinocytosis (Fig. 4e). These results indicate that a reduction in macropinocytic capacity may compromise tumour growth.

The importance of albumin catabolism in human Ras-driven tumours depends on the extent to which the tumours require certain amino acids in excess of the amounts readily attainable in free form from their environment. In human cancers, oncogenic Ras mutations are most common in adenocarcinomas of the pancreas[25,26]. In preliminary metabolomic experiments, we have measured the abundances of 123 known water-soluble metabolites in human pancreatic cancer tumour specimens compared to benign adjacent pancreatic tissue. The most depleted metabolite in pancreatic tumour tissue in comparison to adjacent normal tissue was glutamine, with serine and glycine also decreased (data not shown). A common feature of these amino acids is their consumption in nucleotide synthesis. These preliminary data indicate that human pancreatic tumour tissue is depleted of these free amino acids and raise the possibility that in these depleted conditions, the acquisition of amino acids through macropinocytosis and protein degradation could contribute to tumour growth. In previous experiments investigating human tumour metabolism, it was found that the production of nitrogen waste from some colorectal tumours could be in tenfold excess relative to their uptake of free amino acids[27]. The Ras-induced use of plasma proteins as a source of precursors for macromolecular synthesis and anaplerosis could explain both of these observations, a possibility that remains to be explored in future studies.

Recent years have witnessed a renewed appreciation of the altered metabolic behaviour of tumour cells and the critical role that such metabolic reprogramming has in conferring growth and survival advantages to tumour cells. Here we provide evidence that macropinocytosis-mediated internalization of extracellular protein and its subsequent intracellular degradation may define a mechanism for amino acid supply in Ras-transformed cancer cells. Moreover, these findings

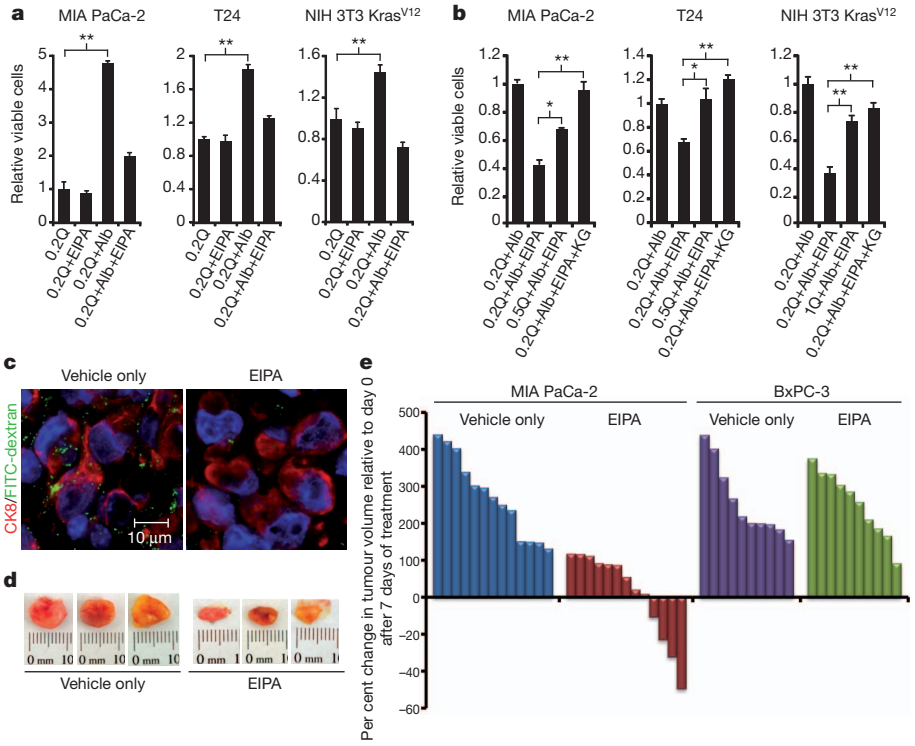

Figure 4 | Macropinocytosis is required for albumin-dependent cancer cell proliferation *in vitro* and for tumour growth *in vivo*. **a**, The compromised proliferation of oncogenic Ras-expressing cells resulting from growth in media containing sub-physiological concentrations of glutamine (0.2 mM, 0.2Q) is reversed by supplementation with 2% albumin (0.2Q + Alb) and this effect is inhibited by treatment with 25 μM EIPA (0.2Q + Alb + EIPA). Total viable cell counts were measured using an MTT assay after 6 days of growth. Data are presented relative to the values obtained for the 0.2Q condition. **b**, The effects of EIPA treatment (25 μM) are suppressed by increasing the glutamine levels in the growth media to the indicated concentrations (that is, 0.5Q indicates 0.5 mM glutamine) or the addition to the medium of 7 mM dimethyl α-ketoglutarate (KG). Data are presented relative to the values obtained for the 0.2Q + Alb condition. For both **a** and **b**, error bars indicate mean ± s.e.m. for $n = 3$ independent experiments. Statistical significance was determined using Student's *t*-test; $^*P < 0.05$, $^{**}P < 0.01$. **c**–**e**, EIPA inhibits macropinocytosis *in vivo* and reduces tumour growth in a subcutaneous heterotopic xenograft model of pancreatic cancer. **c**, Representative images from sections of FITC-dextran (green) injected MIA PaCa-2 tumour xenografts from mice treated with EIPA or vehicle-only controls after 7 days of treatment. The human pancreatic cancer cells are marked by anti-CK8 staining (red). **d**, Representative digital photographs of dissected tumours from mice treated with EIPA or vehicle-only controls. **e**, Waterfall plots indicating the per cent change in tumour volume after 7 days of treatment relative to baseline (day 0 of treatment) for tumours derived from MIA PaCa-2 cells or BxPC-3 cells.

raise the question of whether the inhibition of macropinocytosis can be used for therapeutic targeting in a subset of cancers.

METHODS SUMMARY

Macropinosomes were imaged using an Axiovert 200 inverted fluorescent microscope (Zeiss) and analysed using the 'Analyze Particles' feature in ImageJ (National Institutes of Health). For the heterotopic xenografts, female homozygous NCr nude mice (Taconic) were injected subcutaneously, and when tumours reached an average volume of 500 mm^3 FITC-dextran (Invitrogen) was injected intratumorally. To evaluate the effects of EIPA on macropinocytosis, tumour-bearing mice were treated with EIPA (20 mg ml^{-1}) using an osmotic pump (Alzet, Model 1004) at a pump rate of 0.11 $\mu l\,h^{-1}$. Treatment was initiated when tumours attained an average volume of 50–100 mm^3. As a control, we used animals treated with vehicle only (DMSO in PBS). For tumour growth assays, volumes of the subcutaneous tumours were calculated on the basis of measurements obtained using digital calipers after 7 days of treatment. For the generation of ^{13}C-labelled proteins, a prototrophic haploid SK1 strain of *Saccharomyces cerevisiae* was grown in synthetic complete media lacking amino acids (DIFCO) and containing 2% glucose that was either unlabelled, or uniformly ^{13}C-labelled (Cambridge Isotope Labs). Whole-cell extracts were prepared according to ref. 28. For intracellular metabolite analysis, cell lysate was collected and after extraction, the aqueous phase was collected and evaporated under nitrogen. Gas chromatography/mass spectrometry analysis was performed using an Agilent 6890 GC coupled to a 5975C MS. Mass isotopomer distributions were determined by integrating the appropriate ion fragments and corrected for natural isotope abundance. For glutamine-deprivation assays, cells were cultured in the indicated glutamine concentration and viable cell counts determined using the MTT assay. For some conditions, media was supplemented with BSA (Fraction V, fatty-acid-, nuclease- and protease-free (Calbiochem)). For rescue experiments, dimethyl α-ketoglutarate (Sigma) was used at 7 mM[29]. EIPA (Invitrogen) was diluted in DMSO and used at the indicated concentrations.

Full Methods and any associated references are available in the online version of the paper.

Received 11 July 2012; accepted 2 April 2013.

Published online 12 May; corrected online 29 May 2013 (see full-text HTML version for details).

1. Bar-Sagi, D. & Feramisco, J. R. Induction of membrane ruffling and fluid-phase pinocytosis in quiescent fibroblasts by ras proteins. *Science* **233,** 1061–1068 (1986).
2. Porat-Shliom, N., Kloog, Y. & Donaldson, J. G. A unique platform for H-Ras signaling involving clathrin-independent endocytosis. *Mol. Biol. Cell* **19,** 765–775 (2008).
3. Walsh, A. B. & Bar-Sagi, D. Differential activation of the Rac pathway by Ha-Ras and K-Ras. *J. Biol. Chem.* **276,** 15609–15615 (2001).
4. Lopez-Crapez, E., Chypre, C., Saavedra, J., Marchand, J. & Grenier, J. Rapid and large-scale method to detect K-ras gene mutations in tumor samples. *Clin. Chem.* **43,** 936–942 (1997).
5. Aoki, K., Yoshida, T., Sugimura, T. & Terada, M. Liposome-mediated *in vivo* gene transfer of antisense K-ras construct inhibits pancreatic tumor dissemination in the murine peritoneal cavity. *Cancer Res.* **55,** 3810–3816 (1995).
6. Ivanov, A. I. Pharmacological inhibition of endocytic pathways: is it specific enough to be useful? *Methods Mol. Biol.* **440,** 15–33 (2008).
7. West, M. A., Bretscher, M. S. & Watts, C. Distinct endocytotic pathways in epidermal growth factor-stimulated human carcinoma A431 cells. *J. Cell Biol.* **109,** 2731–2739 (1989).
8. Capon, D. J., Chen, E. Y., Levinson, A. D., Seeburg, P. H. & Goeddel, D. V. Complete nucleotide sequences of the T24 human bladder carcinoma oncogene and its normal homologue. *Nature* **302,** 33–37 (1983).
9. Knowles, M. A. & Williamson, M. Mutation of H-ras is infrequent in bladder cancer: confirmation by single-strand conformation polymorphism analysis, designed restriction fragment length polymorphisms, and direct sequencing. *Cancer Res.* **53,** 133–139 (1993).
10. Wagner, M. *et al.* A murine tumor progression model for pancreatic cancer recapitulating the genetic alterations of the human disease. *Genes Dev.* **15,** 286–293 (2001).
11. Hingorani, S. R. *et al.* Trp53R172H and KrasG12D cooperate to promote chromosomal instability and widely metastatic pancreatic ductal adenocarcinoma in mice. *Cancer Cell* **7,** 469–483 (2005).
12. Nolan-Stevaux, O. *et al. GLI1* is regulated through Smoothened-independent mechanisms in neoplastic pancreatic ducts and mediates PDAC cell survival and transformation. *Genes Dev.* **23,** 24–36 (2009).
13. Stehle, G. *et al.* Plasma protein (albumin) catabolism by the tumor itself–implications for tumor metabolism and the genesis of cachexia. *Crit. Rev. Oncol. Hematol.* **26,** 77–100 (1997).
14. Gaglio, D., Soldati, C., Vanoni, M., Alberghina, L. & Chiaradonna, F. Glutamine deprivation induces abortive s-phase rescued by deoxyribonucleotides in *k-ras* transformed fibroblasts. *PLoS ONE* **4,** e4715 (2009).
15. Matés, J. M. *et al.* Glutamine homeostasis and mitochondrial dynamics. *Int. J. Biochem. Cell Biol.* **41,** 2051–2061 (2009).
16. Reis, R. C., Sorgine, M. H. & Coelho-Sampaio, T. A novel methodology for the investigation of intracellular proteolytic processing in intact cells. *Eur. J. Cell Biol.* **75,** 192–197 (1998).
17. Newsholme, E. A., Crabtree, B. & Ardawi, M. S. Glutamine metabolism in lymphocytes: its biochemical, physiological and clinical importance. *Q. J. Exp. Physiol.* **70,** 473–489 (1985).
18. Wu, M. C., Arimura, G. K. & Yunis, A. A. Mechanism of sensitivity of cultured pancreatic carcinoma to asparaginase. *Int. J. Cancer* **22,** 728–733 (1978).
19. Gaglio, D. *et al.* Oncogenic K-Ras decouples glucose and glutamine metabolism to support cancer cell growth. *Mol. Syst. Biol.* **7,** 523 (2011).
20. Metallo, C. M. *et al.* Reductive glutamine metabolism by IDH1 mediates lipogenesis under hypoxia. *Nature* **481,** 380–384 (2012).
21. Hirai, H. & Varmus, H. E. SH2 mutants of c-src that are host-dependent for transformation are transdominant inhibitors of mouse-cell transformation by activated c-src. *Genes Dev.* **4,** 2342–2352 (1990).
22. Kasahara, K. *et al.* Role of Src-family kinases in formation and trafficking of macropinosomes. *J. Cell. Physiol.* **211,** 220–232 (2007).
23. Mettlen, M. *et al.* Src triggers circular ruffling and macropinocytosis at the apical surface of polarized MDCK cells. *Traffic* **7,** 589–603 (2006).
24. Veithen, A., Cupers, P., Baudhuin, P. & Courtoy, P. J. v-Src induces constitutive macropinocytosis in rat fibroblasts. *J. Cell Sci.* **109,** 2005–2012 (1996).
25. Bos, J. L. ras oncogenes in human cancer: a review. *Cancer Res.* **49,** 4682–4689 (1989).
26. Jones, S. *et al.* Core signaling pathways in human pancreatic cancers revealed by global genomic analyses. *Science* **321,** 1801–1806 (2008).
27. Holm, E. *et al.* Substrate balances across colonic carcinomas in humans. *Cancer Res.* **55,** 1373–1378 (1995).
28. Tsakraklides, V. & Bell, S. P. Dynamics of pre-replicative complex assembly. *J. Biol. Chem.* **285,** 9437–9443 (2010).
29. Wise, D. R. *et al.* Myc regulates a transcriptional program that stimulates mitochondrial glutaminolysis and leads to glutamine addiction. *Proc. Natl Acad. Sci. USA* **105,** 18782–18787 (2008).

Supplementary Information is available in the online version of the paper.

Acknowledgements We are grateful to members of the Bar-Sagi laboratory for their comments and discussions, and N. Fehrenbacher and M. Philips for sharing cell lines. This work was supported National Institutes of Health (NIH) grant R01CA055360 to D.B.-S. C.C. was supported by a Canadian Institutes of Health Research postdoctoral fellowship and an AACR postdoctoral fellowship provided by the Pancreatic Cancer Action Network. M.G.V.H. acknowledges support from the Burroughs Wellcome Fund, the Damon Runyon Cancer Research Foundation, the Smith Family, the Stern family, the Broad Institute and the National Cancer Institute (P01-CA117969 and P30-CA14051-39). J.J.K. was supported by a Hope Funds for Cancer Research Fellowship (HFCR-11-03-01). C.B.T., J.A.D. and J.D.R. acknowledge support by the Stand Up To Cancer (SU2C) Pancreatic Cancer Dream Team Award. All animal care and procedures were approved by the Institutional Animal Care and Use Committee at NYU School of Medicine. The Histopathology Core of NYU School of Medicine is partially supported by the National Institutes of Health (grant 5 P30CA016087-32). Troma I, an antibody that recognizes CK8, was contributed by P. Brulet and R. Kemler and made available by the Developmental Studies Hybridoma Bank under the auspices of the NICHD.

Author Contributions C.C. and D.B.-S. conceived the cell biological and cell-growth experiments. C.C. carried out the macropinocytic assays, microscopy and proliferation assays. C.C. and R.G.S.-A. carried out the xenograft experiments. C.C. and E.G. carried out the KRAS knockdown experiments. S.M.D., S.J.P., C.M.M. and M.G.V.H. conceived and carried out the ^{13}C-labelling experiments. J.J.K., S.H., M.N., J.A.D., C.B.T. and J.D.R. conceived and carried out the human metabolomics analysis.

Author Information Reprints and permissions information is available at www.nature.com/reprints. The authors declare no competing financial interests. Readers are welcome to comment on the online version of the paper. Correspondence and requests for materials should be addressed to D.B.-S. (dafna.bar-sagi@nyumc.org).

METHODS

Cell culture. All cells were maintained under 5% CO_2 at 37 °C in medium supplemented with 10% FBS (Gibco). MIA PaCa-2 and T24 cells were maintained in DMEM (Invitrogen); BxPC-3 and 5637 cells were maintained in RPMI (Gibco) supplemented with 1 mM sodium pyruvate (CellGro) and NIH 3T3 cells were maintained in DMEM supplemented with 1× MEM non-essential amino acids (Sigma).

Macropinosome visualization and quantification. Cells were seeded onto glass coverslips. Twenty-four to forty-eight hours after cell seeding, cells were serum starved for 18 h. Macropinosomes were marked using a high-molecular-mass TMR-dextran (Invitrogen)-uptake assay wherein TMR-dextran was added to serum-free medium at a final concentration of 1 mg ml^{-1} for 30 min at 37 °C. At the end of the incubation period, cells were rinsed five times in cold PBS and immediately fixed in 3.7% formaldehyde. Cells were DAPI-treated to stain nuclei and coverslips mounted onto slides using DAKO Mounting Media (DAKO). Images were captured using an Axiovert 200 inverted fluorescent microscope (Zeiss) and analysed using the 'Analyze Particles' feature in ImageJ (National Institutes of Health). The total particle area per cell was determined from at least five fields that were randomly selected from different regions across the entirety of each sample.

Interference RNA-mediated knockdown of KRAS. KRAS knockdown was achieved through the pTRIPZ doxycycline-inducible short hairpin RNA (shRNA) expression lentivirus system (Open Biosystems). shRNA sequences for scramble shRNA (5′-GGAAGTGCAATTATTCTATTA-3′) and *KRAS* shRNA 1 (5′-TAGTTGGAGCTTGTGGCGTAG-3′) were cloned into pTRIPZ according to the manufacturer's protocol. The *KRAS* shRNA 2 construct was purchased from Open Biosystems. MIA PaCa-2 cells were transduced with lentiviral particles containing the indicated pTRIPZ scramble shRNA or *KRAS* shRNAs and selected with 2 μg ml^{-1} puromycin (Calbiochem) for 3 days. shRNA expression was induced with 1 μg ml^{-1} doxycycline and efficient knockdown was confirmed by immunoblotting with KRAS-specific antibodies (sc-30, Santa Cruz Biotechnology).

Mice. For the heterotopic xenografts, female homozygous NCr nude mice (Taconic) were injected subcutaneously in both flanks at 8 weeks of age with 1×10^6 cells mixed at a 1:1 dilution with BD Matrigel (BD Biosciences) in a total volume of 100 μl. When tumours reached an average volume of 500 mm^3, 1 mg of fixable FITC-dextran (Invitrogen) diluted in PBS to a volume of 100 μl was injected intratumorally. At 2 h post-injection, tumours were removed and rapidly frozen in tissue-freezing medium. Experimental cohorts of at least three mice per pancreatic cancer cell line, each mouse implanted in both flanks, were used in triplicate experiments. To quantify FITC-dextran uptake in the tumours, the total particle area per cell was determined from at least five sections per tumour with five fields analysed per section, totalling at least 15 randomly selected fields per tumour.

For the autochthonous model, pancreata from *P48-cre; lsl-Kras^{G12D}; Trp53$^{-/+}$* (KPC) mice, at 12 weeks of age, were injected with 2 mg of FITC-dextran and subsequently collected. As a control, we analysed pancreatic tissue from wild-type mice. Frozen sections from sectioned pancreata were analysed using standard microscopic techniques and macropinocytosis-positive cells were identified by the visualization of FITC-positive puncta.

To evaluate the effects of EIPA on macropinocytosis *in vivo*, mice heterotopically transplanted with MIA PaCa-2 cells, as described above, were treated with an osmotic pump (Alzet) when tumours attained an average volume of 50–100 mm^3 (approximately 2 weeks after transplantation). EIPA (20 mg ml^{-1} in a 1:4 dilution of DMSO and PBS) was administered at a pump rate of 0.11 μl h^{-1}. As a control, we used animals treated with vehicle only (DMSO in PBS). Animals were intratumorally injected with FITC-dextran at various time points (4–7 days) during the course of treatment. After a subsequent 1-h time interval, tumours were collected, sectioned and analysed using standard microscopic techniques. Each experimental group consisted of five animals and at least five sections per pancreas were analysed.

For tumour growth assays, the animals were randomized into control and treated groups. Treatment, as described above, was initiated 2 weeks post-transplantation when the tumours had attained an average volume of 50–100 mm^3. Volumes of the subcutaneous tumours were calculated on the basis of measurements obtained in a blinded fashion using digital calipers after 7 days of treatment.

Metabolite quantification. NIH 3T3 Kras^{V12} cells were grown in DMEM with/without the supplementation of 2% BSA for 24 h before collection. Cells were lysed in a buffered 1% Triton solution and lysates were de-proteinized using perchloric acid-precipitation (BioVision). Relative metabolite concentrations were then determined using colorimetric assay kits: glutamate/glutamine (Bioassay Systems) and α-ketoglutarate (BioVision).

Generation of ^{13}C-labelled proteins. A prototrophic haploid SK1 strain of *Saccharomyces cerevisiae* was grown to an attenuance of 4.0 in synthetic complete media lacking amino acids (DIFCO) and containing 2% glucose that was either normal isotopic, or uniformly ^{13}C-labelled (Cambridge Isotopes). Whole-cell extracts were prepared according to ref. 28. In brief, cells were collected, re-suspended in 100 mM HEPES, pH 7.6, 0.8 mM sorbitol, 10 mM magnesium acetate, 2 mM EDTA and 300 mM potassium glutamate and lysed using a Sample Prep 6870 Freezer/Mill (SPEX CertiPrep). Lysate was treated with DNase (Ambion) and RNaseH (Invitrogen) and dialysed against PBS. Endogenous protease and glutaminase activity were eliminated by adding the protein to FBS and incubating for 30 min at 56 °C. The resulting labelled and unlabelled protein was either: (1) tagged with N-hydroxysuccinimide-rhodamine (Pierce) according to manufacturer's instructions for visualization in confocal microscopy experiments, or (2) used to supplement cell culture media for subsequent tracing experiments.

Metabolite extraction. For extracellular metabolite analysis, media was collected and metabolites extracted using 0.3 ml ice-cold acetone containing 1 μg norvaline. Extracts clarified by centrifugation and the supernatant evaporated under nitrogen. For intracellular metabolite analysis, cells were rinsed three times with cold saline and quenched with cold methanol. One half volume of cold water containing 1 μg norvaline was added, cell lysate was collected, and one volume of chloroform was added to each sample. After extraction the aqueous phase was collected and evaporated under nitrogen.

Gas chromatography/mass spectrometry (GC/MS) analysis. Dried polar metabolites were dissolved in 20 μl of 2% methoxyamine hydrochloride in pyridine (Thermo) and held at 37 °C for 1.5 h. After dissolution and reaction, tert-butyldimethylsilyl derivatization was initiated by adding 30 μl *N*-methyl-*N*-(tert-butyldimethylsilyl)trifluoroacetamide + 1% tert-butyldimethylchlorosilane (Regis) and incubating at 37 °C for 1 h. GC/MS analysis was performed using an Agilent 6890 GC equipped with a 30m DB-35MS capillary column connected to an Agilent 5975B MS operating under electron impact ionization at 70 eV. One microlitre of sample was injected in splitless mode at 270 °C, using helium as the carrier gas at a flow rate of 1 ml min^{-1}. For measurement of amino acids, the GC oven temperature was held at 100 °C for 3 min and increased to 300 °C at 3.5 °C min^{-1}. The MS source and quadrupole were held at 230 °C and 150 °C, respectively, and the detector was run in scanning mode, recording ion abundance in the range of 100–605 *m*/*z*. MIDs were determined by integrating the appropriate ion fragments[30] listed in Supplementary Table 1 and corrected for natural isotope abundance using in house algorithms adapted from ref. 31.

Glutamine-deprivation assays. Cells were plated in 96-well plate format at a density of 1,000–1,500 cells per well. Thirty-two hours after seeding, cells were rinsed briefly in PBS and incubated in the indicated glutamine-deprivation media. Glutamine-free DMEM media was supplemented to the indicated concentration of glutamine in the presence of 10% dialysed FBS and 25 mM HEPES. For some conditions, media was supplemented with BSA (Fraction V, fatty-acid-, nuclease- and protease-free, Calbiochem). The nominal 0.2% albumin concentration inherently present in complete media was supplemented such that the final concentration of BSA in the media was 2%. For rescue experiments, dimethyl α-ketoglutarate (Sigma) was used at 7 mM[29]. For all experiments, media was replaced every 24 h. Viable cell counts were obtained using the MTT assay and relative cell number was determined by Syto 60 staining. EIPA (Invitrogen) was diluted in DMSO and used at the indicated concentrations with vehicle-only controls consisting of DMSO alone. Images depicting cell number in 96-well format were obtained by staining with Syto 60 (Molecular Probes), a red fluorescent nucleic acid stain. Plates were then scanned with an Odyssey Imager (LI-COR) at 700 nm.

30. Antoniewicz, M. R., Kelleher, J. K. & Stephanopoulos, G. Accurate assessment of amino acid mass isotopomer distributions for metabolic flux analysis. *Anal. Chem.* **79,** 7554–7559 (2007).
31. Fernandez, C. A., Des Rosiers, C., Previs, S. F., David, F. & Brunengraber, H. Correction of 13C mass isotopomer distributions for natural stable isotope abundance. *J. Mass Spectrom.* **31,** 255–262 (1996).